

Analysis of Optical Single Sideband Modulators for Radio Over Fiber Link with and without Second Order Sidebands

Pooja GOEL , Rahul KAUSHIK 

Department of Electronics and Communication Engineering, Jaypee Institute of Information Technology, A-10, Sector-62, 201 309 Noida, Uttar Pradesh, India

pooja.goel.leo@gmail.com, rahul.kaushik@jiit.ac.in

DOI: 10.15598/aece.v19i4.4203

Article history: Received Apr 13, 2021; Revised Jul 25, 2021; Accepted Jul 27, 2021; Published Dec 31, 2021. This is an open access article under the BY-CC license.

Abstract. *The analysis of Optical Single Sideband (OSSB) generation with and without second-order sidebands for Radio over Fiber (RoF) is presented. The performance of systems based on hybrid coupler with distinct phase angle and Dual-Parallel Dual-Drive Mach-Zehnder Modulator (DP-DDMZM) is compared using simulation. Impact of parameters like Single-Mode Fiber (SMF) length, Radiofrequency (RF) amplitude, and laser linewidth on Signal-to-Noise Ratio (SNR) has been investigated. It has been observed that eliminating one of the second-order sidebands with 120° hybrid coupler improves peak SNR in comparison to 90° hybrid coupler with both second-order sidebands and DP-DDMZM-based system without second-order sidebands irrespective of Continuous Wave (CW) laser linewidth.*

Keywords

Dual Drive Mach Zehnder Modulator, Dual Parallel Dual Drive Mach Zehnder Modulator, Optical Single Sideband, Radio over Fiber.

1. Introduction

Radio over Fiber (RoF) is a technique, in which Radiofrequency (RF) signals are transmitted over optical fiber. The RoF combines the advantage of abundant bandwidth of optical fiber with wireless mobility and flexibility for various broadband applications [1]. Two methods for intensity modulation are used. Direct intensity modulation is less complex and cost-

effective but provides good performance up to several GHz [2]. For high-performance RoF links, external intensity modulation is preferred. The external modulation techniques such as Double Sideband Suppressed Carrier (DSBSC), Double Sideband Full Carrier (DSBFC), Single Sideband (SSB) and Vestigial Sideband (VSB) are gaining interest in research community. Optical Single Sideband (OSSB) has many advantages compared to Double Sideband (DSB). The OSSB is preferred for long-haul applications with lower number of repeaters and hence reduces system complexity and cost [3] and [4]. Moreover, it leads to reduced power fading and interference by cancelling harmonics [5]. Various methods for implementation of OSSB RoF systems are proposed in the literature. The OSSB system using fiber Bragg grating based on Hilbert transform has been proposed in [6]. This scheme has relatively poor long-term stability due to wavelength drifting. The OSSB RoF transmission system based on 90° phase shifter has been analyzed in [7]. The OSSB modulation based on Dual-Drive Mach-Zehnder Modulator (DD-MZM) and 120° hybrid coupler has been proposed in [8] and it was shown that suppression of one of the second-order sidebands, either (+2nd) or (-2nd), improves the OSSB performance compared to OSSB generation using 90° hybrid coupler. Two OSSB systems based on distinct hybrid coupler have been compared in [9]. In the [10] was proposed OSSB modulation without second-order sidebands ($\pm 2nd$) based on Dual-Parallel Dual-Drive Mach-Zehnder Modulator (DP-DDMZM). For long-haul transmission, high Signal-to-Noise Ratio (SNR) is required. The SNR can be improved either by increasing transmitted signal power or reducing the noise. But as signal power increases, modulation index of MZM also increases. With increase in modula-

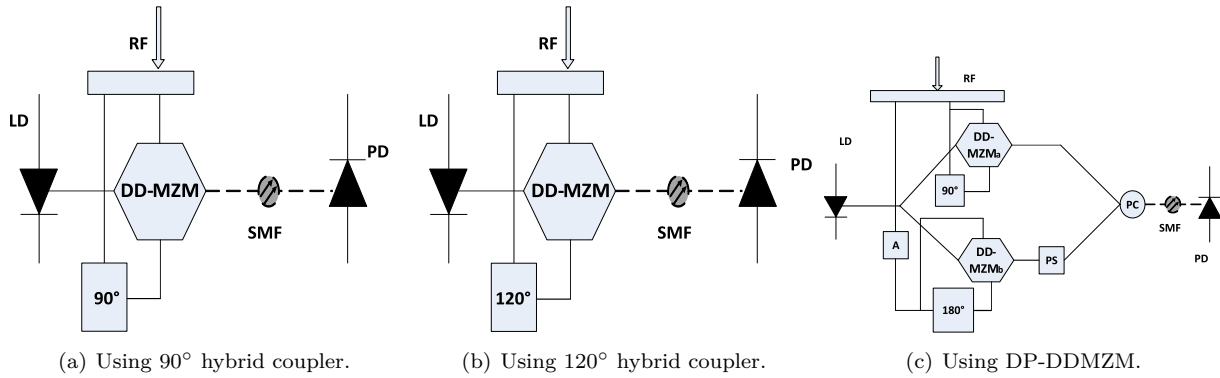


Fig. 1: Block diagrams of OSSB generation with and without second-order sidebands [LD: Laser Diode, PC: Power Coupler, PD: Photodiode, RF: Radiofrequency, PS: Phase Shift, A: Attenuator, SMF: Single-Mode Fiber].

tion index, power of higher-order harmonics strengthens which causes power fading due to chromatic dispersion. To overcome chromatic dispersion and power fading at the receiver, it is required to eliminate one of the second-order sidebands, either upper or lower, but not both second-order sidebands, which also increases transmission distance [11] and [12]. Thus, it would be significant to analyze the performance of OSSB systems with and without second-order sidebands. However, the comparison of OSSB generation based on the distinct phase angle of hybrid coupler and DP-DDMZM has not been carried out in any of these studies.

This work aims to analyze RoF systems, employing OSSB generation using hybrid couplers and DP-DDMZM. Further, the performance of the RoF system depends on various parameters like input RF signal, laser linewidth and optical fiber length. It would be of critical importance to analyze the performance of the systems against these parameters. In this work, OSSB generation with and without second-order sidebands for RoF is presented. Theoretical analysis has been done and simulation verification has been conducted to compare the performance of different OSSB modulators with and without second-order sidebands. The SNR variations due to various parameters like optical fiber length, RF amplitude and laser linewidth in different OSSB modulators have also been investigated.

Rest of the paper is organized as follows. Section 2. presents the proposed system models for OSSB generation using 90° hybrid coupler, 120° hybrid coupler, and DP-DDMZM followed by theoretical analysis. Section 3. describes the results in which, the influence of optical fiber length (km), RF amplitude and laser linewidth on SNR has been analyzed and discussed, and Sec. 4. concludes the paper.

2. System Models Theory

The implementation of OSSB RoF systems with and without second-order sidebands, based on DD-MZM and DP-DDMZM are shown in Fig. 1. An OSSB signal can be generated using DD-MZM with 90° or 120° hybrid couplers and by using DP-DDMZM. The output signals from laser diode and RF oscillator can be represented as:

$$x_L(t) = A_o \exp j(\omega_L t + \phi_L(t)), \tag{1}$$

where A_o , ω_L and $\phi_L(t)$ represent amplitude, angular frequency, and phase noise of laser, respectively.

$$x_R(t) = V_{RF} \cos(\omega_{RF} t + \phi_{RF}(t)). \tag{2}$$

Similarly, V_{RF} , ω_{RF} and ϕ_{RF} represent amplitude, angular frequency, and phase noise of RF oscillator, respectively. The output at DD-MZM [9] can be represented as:

$$V_o = \frac{A_o \alpha}{2} \left[\exp j \left[\begin{matrix} \omega_L t + \gamma \pi + \phi_L(t) + \\ \mu \cos(\omega_{RF} t + \phi_{RF}(t)) \end{matrix} \right] + \exp j \left[\begin{matrix} \omega_L t + \phi_L(t) + \\ \mu \cos(\omega_{RF} t + \phi_{RF}(t) + \theta) \end{matrix} \right] \right], \tag{3}$$

where α is insertion loss, γ is normalized bias voltage and μ is modulation index. For generating OSSB signal using 90° hybrid coupler, $\gamma = \frac{1}{2}$ and $\theta = \frac{\pi}{2}$. Therefore, the output voltage can be expressed as:

$$V_{90^\circ} = \frac{A_o \alpha}{2} \left[\exp j \left[\begin{matrix} \omega_L t + \frac{1}{2} \pi + \phi_L(t) + \\ \mu \cos(\omega_{RF} t + \phi_{RF}(t)) \end{matrix} \right] + \exp j \left[\begin{matrix} \omega_L t + \phi_L(t) + \\ \mu \cos(\omega_{RF} t + \phi_{RF}(t) + \frac{\pi}{2}) \end{matrix} \right] \right]. \tag{4}$$

According to Jacobi-Anger identity, $e^{iz \cos \theta} = \sum_{-\infty}^{\infty} i^n J_n(z) e^{in\theta}$ where $J_n(z)$ is n^{th} order Bessel function of the first kind. Using this

identity, the Eq. (4) can be rewritten as:

$$V_{90^\circ} = \frac{A_o\alpha}{2} \left[\sum_{n=-\infty}^{\infty} (j)^n J_n(\mu) \exp j \left[\omega_L t + \frac{\pi}{2} + \phi_L(t) + (n\omega_{RF}t + n\phi_{RF}(t)) \right] + \sum_{n=-\infty}^{\infty} (j)^n J_n(\mu) \exp j \left[\omega_L t + \phi_L(t) + \left(n\omega_{RF}t + n\phi_{RF}(t) + \frac{n\pi}{2} \right) \right] \right]. \quad (5)$$

Expanding Eq. (5) up-to second order terms, the output signals can be represented as:

$$V_{90^\circ} = A_o\alpha \left[\frac{1}{\sqrt{2}} J_0(\mu) \exp j \left(\omega_L t + \phi_L(t) + \frac{\pi}{4} \right) - J_1(\mu) \exp j \left(\omega_L t + \phi_L(t) + \omega_{RF}t + \phi_{RF}(t) \right) + \frac{1}{\sqrt{2}} J_2(\mu) \exp j \left(\omega_L t + \phi_L(t) + 2\omega_{RF}t + 2\phi_{RF}(t) - \frac{\pi}{4} \right) + \frac{1}{\sqrt{2}} J_{-2}(\mu) \exp j \left(\omega_L t + \phi_L(t) - 2\omega_{RF}t - 2\phi_{RF}(t) - \frac{\pi}{4} \right) \right]. \quad (6)$$

It is seen from Eq. (6), that output spectrum consists of carrier, +1st -order sideband and both ± 2 nd -order sidebands, while -1st -order sideband is suppressed. Similarly, for generating OSSB signal using 120° hybrid coupler, $\gamma = \frac{1}{3}$ and $\theta = \frac{2\pi}{3}$. Therefore, the output voltage can be expressed as:

$$V_{120^\circ} = \frac{A_o\alpha}{2} \left[\exp j \left[\omega_L t + \frac{1}{3}\pi + \phi_L(t) + \mu \cos(\omega_{RF}t + \phi_{RF}(t)) \right] + \exp j \left[\omega_L t + \phi_L(t) + \mu \cos \left(\omega_{RF}t + \phi_{RF}(t) + \frac{2\pi}{3} \right) \right] \right]. \quad (7)$$

Using Jacobi-Anger identity, Eq. (7) can be rewritten as:

$$V_{120^\circ} = \frac{A_o\alpha}{2} \left[\sum_{n=-\infty}^{\infty} (j)^n J_n(\mu) \exp j \left[\omega_L t + \frac{\pi}{3} + \phi_L(t) + (n\omega_{RF}t + n\phi_{RF}(t)) \right] + \sum_{n=-\infty}^{\infty} (j)^n J_n(\mu) \exp j \left[\omega_L t + \phi_L(t) + \left(n\omega_{RF}t + n\phi_{RF}(t) + \frac{n2\pi}{3} \right) \right] \right]. \quad (8)$$

$$V_{120^\circ} = A_o\alpha \left[\frac{\sqrt{3}}{2} J_0(\mu) \exp j \left(\omega_L t + \phi_L(t) + \frac{\pi}{6} \right) - \frac{\sqrt{3}}{2} J_1(\mu) \exp j \left(\omega_L t + \phi_L(t) + \omega_{RF}t + \phi_{RF}(t) \right) + j \frac{\sqrt{3}}{2} J_{-2}(\mu) \exp j \left(\omega_L t + \phi_L(t) - 2\omega_{RF}t - 2\phi_{RF}(t) \right) \right]. \quad (9)$$

It may be noted from Eq. (9) that output spectrum consists of carrier, +1st -order sideband and -2nd -order sidebands while, +2nd -order sideband and -1st -order sidebands are suppressed. OSSB modulator using DP-DDMZM without second order sidebands is shown in Fig. 1(c). This OSSB generation is based on two DDMZM operating in parallel mode [10]. So the net output field can be expressed as:

$$V_{\text{DP-DDMZM}} = V_{\text{DDMZMa}} + V_{\text{DDMZMb}}. \quad (10)$$

Here, V_{DDMZMa} is operated as SSB modulator with $\gamma = \frac{1}{2}$ and $\theta = \frac{\pi}{2}$ while V_{DDMZMb} is biased at Maximum Transmission Bias Point (MATBP) with $\gamma = 0$ and $\theta = \pi$.

$$V_{\text{DDMZMa}} = A_o\alpha \left[\frac{1}{\sqrt{2}} J_0(\mu) \exp j \left(\omega_L t + \phi_L(t) + \frac{\pi}{4} \right) - J_1(\mu) \exp j \left(\omega_L t + \phi_L(t) + \omega_{RF}t + \phi_{RF}(t) \right) + \frac{1}{\sqrt{2}} J_2(\mu) \exp j \left(\omega_L t + \phi_L(t) + 2\omega_{RF}t + 2\phi_{RF}(t) - \frac{\pi}{4} \right) + \frac{1}{\sqrt{2}} J_{-2}(\mu) \exp j \left(\omega_L t + \phi_L(t) - 2\omega_{RF}t - 2\phi_{RF}(t) - \frac{\pi}{4} \right) \right]. \quad (11)$$

$$V_{\text{DDMZMb}} = A_o\alpha \left[J_0(\beta\mu) \exp j \left(\omega_L t + \phi_L(t) \right) + J_2(\beta\mu) \exp j \left(\omega_L t + \phi_L(t) + 2\omega_{RF}t + 2\phi_{RF}(t) \right) + J_{-2}(\beta\mu) \exp j \left(\omega_L t + \phi_L(t) - 2\omega_{RF}t - 2\phi_{RF}(t) \right) \right]. \quad (12)$$

where β is the attenuation of attenuator. Considering the $\frac{3\pi}{4}$ phase shift introduced by phase shifter, the output at V_{DDMZMb} is given by:

$$V_{\text{DDMZMb}} = A_o\alpha \left[J_0(\beta\mu) \exp j \left(\omega_L t + \phi_L(t) + \frac{3\pi}{4} \right) + J_2(\beta\mu) \exp j \left(\omega_L t + \phi_L(t) + 2\omega_{RF}t + 2\phi_{RF}(t) + \frac{3\pi}{4} \right) + J_{-2}(\beta\mu) \exp j \left(\omega_L t + \phi_L(t) - 2\omega_{RF}t - 2\phi_{RF}(t) + \frac{3\pi}{4} \right) \right]. \quad (13)$$

Now, using Eq. (10), the net optical field for DP-DDMZM can be obtained as:

$$V_{\text{DP-DDMZM}} = A_0 \alpha \left[\left[\sqrt{\left(\frac{1}{\sqrt{2}} J_0(\mu)\right)^2 + J_0(\beta\mu)^2} \right] \cdot \exp j \left(\omega_L t + \phi_L(t) + \frac{3\pi}{4} \right) - J_1(\mu) \exp j \left(\omega_L t + \phi_L(t) + \omega_{RF} t + \phi_{RF}(t) \right) \right]. \quad (14)$$

From Eq. (14), it may be observed that both $\pm 2\text{nd}$ -order sidebands have same magnitude so that they will cancel out and we get carrier and 1st-order sideband. Both second order sidebands are suppressed. After transmission on SMF over distance L (km), the signals can be mathematically represented as:

$$V_{90^\circ} = A_0 \alpha 10^{-\frac{\alpha_F L}{20}} \left[\frac{1}{\sqrt{2}} J_0(\mu) \exp j \left(\omega_L t + \phi_L(t - t'_0) + \frac{\pi}{4} - \phi_1 \right) - J_1(\mu) \exp j \left(\omega_L t + \phi_L(t - t'_1) + \omega_{RF} t + \phi_{RF}(t - t'_1) - \phi_2 \right) + \frac{1}{\sqrt{2}} J_2(\mu) \exp j \left(\omega_L t + \phi_L(t - t'_2) + 2\omega_{RF} t + 2\phi_{RF}(t - t'_2) - \frac{\pi}{4} - \phi_3 \right) + \frac{1}{\sqrt{2}} J_{-2}(\mu) \exp j \left(\omega_L t + \phi_L(t - t'_2) - 2\omega_{RF} t - 2\phi_{RF}(t - t'_2) - \frac{\pi}{4} - \phi_3 \right) \right], \quad (15)$$

where α_F denotes fiber loss, t'_0 , t'_1 , and t'_2 denote group delay for central angular laser frequency ω_L , an upper sideband of $\omega_L + \omega_{RF}$ and $\omega_L \pm \omega_{RF}$. ϕ_1 , ϕ_2 , ϕ_3 are phase shifts due to dispersion. Similarly, for OSSB using 120° hybrid coupler and DP-DDMZM, the output voltages can be expressed as:

$$V_{120^\circ} = A_0 \alpha 10^{-\frac{\alpha_F L}{20}} \left[\frac{\sqrt{3}}{2} J_0(\mu) \exp j \left(\omega_L t + \phi_L(t - t'_0) + \frac{\pi}{6} - \phi_1 \right) - \frac{\sqrt{3}}{2} J_1(\mu) \exp j \left(\omega_L t + \phi_L(t - t'_1) + \omega_{RF} t + \phi_{RF}(t - t'_1) - \phi_2 \right) + j \frac{\sqrt{3}}{2} J_{-2}(\mu) \exp j \left(\omega_L t + \phi_L(t - t'_2) + 2\omega_{RF} t + 2\phi_{RF}(t - t'_2) - \phi_3 \right) \right], \quad (16)$$

$$V_{\text{DP-DDMZM}} = A_0 \alpha 10^{-\frac{\alpha_F L}{20}} \left[\left[\sqrt{\left(\frac{1}{\sqrt{2}} J_0(\mu)\right)^2 + J_0(\beta\mu)^2} \right] \cdot \exp j \left(\omega_L t + \phi_L(t - t'_0) + \frac{3\pi}{4} - \phi_1 \right) - J_1(\mu) \exp j \left(\omega_L t + \phi_L(t - t'_1) + \omega_{RF} t + \phi_{RF}(t - t'_1) - \phi_2 \right) \right]. \quad (17)$$

Using square law model, the photocurrent $i_{(90^\circ)}$ can be calculated as $i_{(90^\circ)} = R |V_{(90^\circ)}|^2$. Hence,

$$i_{(90^\circ)} = R A_1^2 \left[B - \sqrt{2} a_1 \cos \left(\omega_{RF} t + \phi_{RF}(t - t'_1) - \phi_2 - \phi_L(t - t'_0) + \phi_L(t - t'_1) - \frac{\pi}{4} + \phi_1 \right) + 2a_2 \cos \left(2\omega_{RF} t - \phi_L(t - t'_0) + \phi_1 - \phi_L(t - t'_2) + 2\phi_{RF}(t - t'_2) - \phi_3 - \frac{\pi}{2} \right) - \frac{2\sqrt{2} J_1(\mu) J_2(\mu)}{J_0(\mu)^2} \cdot \cos \left(\omega_{RF} t - \left(\phi_L(t - t'_1) - \phi_L(t - t'_2) + \phi_{RF}(t - t'_1) + \omega_{RF} t - \phi_2 + \phi_3 + \frac{\pi}{4} \right) \right) \right], \quad (18)$$

where R is the responsivity of photodiode,

$$B = \frac{1}{2} + \alpha_1^2 + \alpha_2^2, \quad \alpha_1 = \frac{J_1(\mu)}{J_0(\mu)}, \quad \alpha_2 = \frac{J_2(\mu)}{J_0(\mu)},$$

$$A_1 = A_0 \alpha 10^{-\frac{\alpha_F L}{20}} J_0(\mu).$$

$$i_{(120^\circ)} = R A_1^2 \left[B' - \frac{3}{2} a_1 \cos \left(\omega_{RF} t + \phi_{RF}(t - t'_1) - \phi_2 - \phi_L(t - t'_0) + \phi_L(t - t'_1) - \frac{\pi}{6} + \phi_1 \right) + \frac{3}{2} a_2 \cos \left(2\omega_{RF} t - \phi_L(t - t'_0) + \phi_1 - \phi_L(t - t'_2) + 2\phi_{RF}(t - t'_2) - \phi_3 - \frac{\pi}{6} \right) - \frac{3J_1(\mu) J_2(\mu)}{2J_0(\mu)^2} \cdot \cos \left(\omega_{RF} t - \left(\phi_L(t - t'_1) - \phi_L(t - t'_2) + \phi_{RF}(t - t'_1) + \omega_{RF} t - \phi_2 + \phi_3 + \frac{\pi}{6} \right) \right) \right], \quad (19)$$

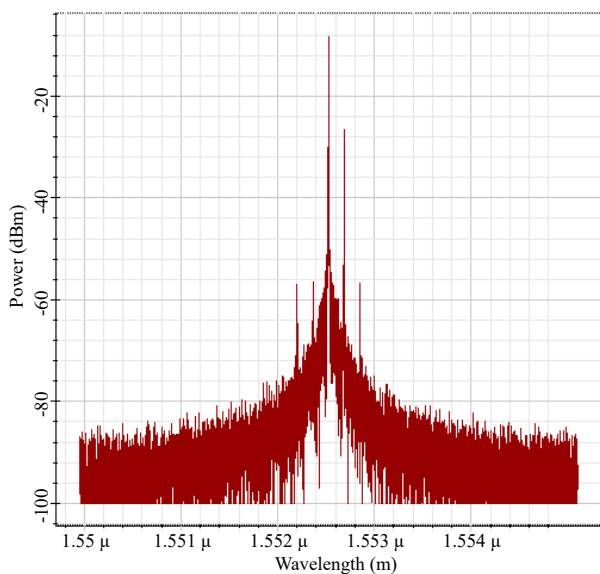
where $B' = \frac{3}{2} + \frac{3}{4} \alpha_1^2 + \frac{3}{4} \alpha_2^2$.

$$i_{(\text{DP-DDMZM})} = R A_1^2 \left[k^2 + \alpha_1^2 + 2k\alpha_1 \cos \left(\omega_{RF} t + \phi_{RF}(t - t'_1) - \phi_2 - \phi_L(t - t'_0) + \phi_L(t - t'_1) - \frac{3\pi}{4} + \phi_1 \right) \right], \quad (20)$$

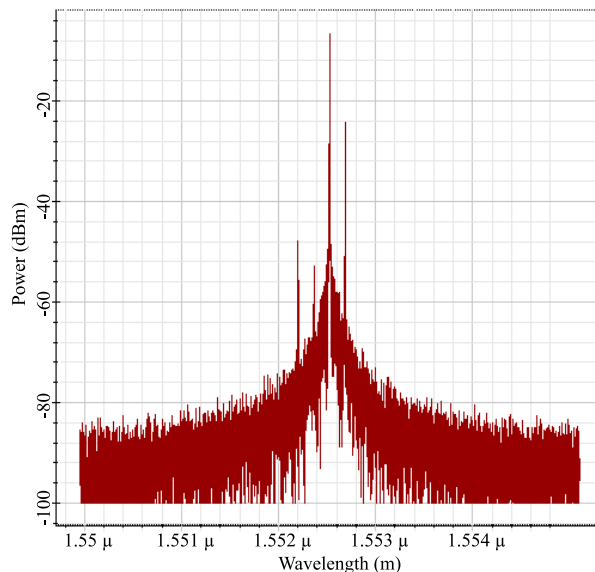
where $k = \frac{\sqrt{\left(\frac{1}{\sqrt{2}}J_0(\mu)\right)^2 + J_0(\beta\mu)^2}}{J_0(\mu)}$. Autocorrelation function $R_l(\tau) = \langle i(t)i(t+\tau) \rangle$ is related to power spectral density by $S_l(f) = F\langle R_l(\tau) \rangle$ where F is Fourier transform. The SNR is related to receive power which is directly proportional to power spectral density as $P_{rc} = \int_{F_{RF}-B_{RF}}^{F_{RF}+B_{RF}} S_l(f)$, where F_{RF} is signal frequency and B_{RF} denotes filter bandwidth. Hence, it is seen that SNR is a function of RF input signal, optical fiber length, bandwidth, and phase noise of laser and RF oscillator.

3. Results and Discussion

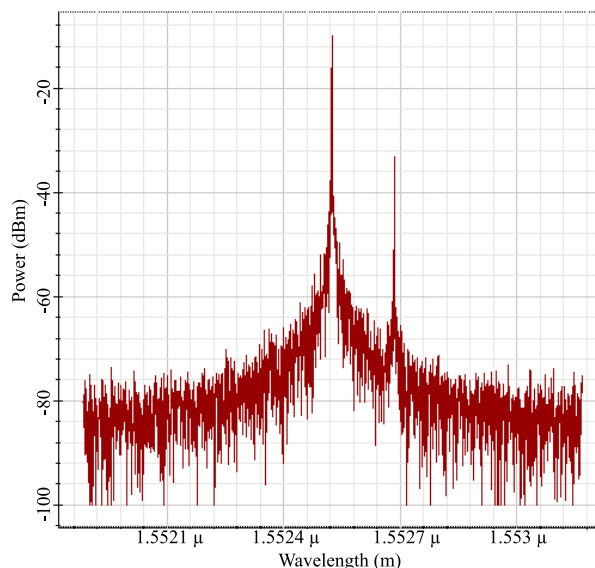
In this section, the performance of OSSB modulators shown in Fig. 1 is compared and analyzed. For this study, systems are simulated using OptiSystem 16.0. OptiSystem is an optical communication simulation package based on realistic modelling of fiber-optic systems. The simulation parameters, remaining constant throughout this work, are shown in Tab. 1. The simulated optical spectra for OSSB modulators with and without second-order sidebands are shown in Fig. 2. The output spectrum for OSSB generation using 90° hybrid coupler is shown in Fig. 2(a). It can be seen that spectrum consists of carrier, +1st-order sideband and both ±2nd-order sidebands while -1st-order sideband is suppressed. Similarly, the output spectrum for OSSB generation using 120° hybrid coupler is shown in Fig. 2(b).



(a) Using 90° hybrid coupler (with both ±2nd -order sidebands).



(b) Using 120° hybrid coupler (with -2nd -order sidebands).



(c) Using DP-DDMZM (without ±2nd -order sidebands).

Fig. 2: Spectra of OSSB Modulators with and without second-order sidebands.

Tab. 1: Simulation parameters.

Parameter	Value
Sine Generator frequency	20 GHz
CW Laser frequency	193.1 THz
Power of laser	0 dBm
LiNb Mach-Zehnder Modulator Extinction Ratio	30 dB
Bias Voltage, V_π	4 V
Optical fiber length	0–120 km
Fiber attenuation	0.2 dB·km ⁻¹
Fiber Dispersion	16.75 (ps·nm ⁻¹)·km ⁻¹
CW laser width	0–700 MHz
APD Gain	3
Responsivity	1 A·W ⁻¹

One can see that output spectrum consists of carrier, +1st -order sideband and -2nd -order sidebands, while +2nd -order sideband and -1st -order sidebands are suppressed. The spectrum of OSSB modulator using DP-DDMZM is shown in Fig. 2(b). Here, both the ± 2 nd -order sidebands have same magnitude so that they cancel out and the spectrum consists of carrier and first-order sideband.

The variation of received SNR with optical fiber length (km) for OSSB generation using 90°, 120° hybrid coupler and DP-DDMZM is shown in Fig. 3. These plots are obtained at fixed RF amplitude of 0.22 and 10 MHz CW laser linewidth. Results show that SNR decreases as SMF length increases. It may also be noted that OSSB generation using 120° hybrid coupler is giving better performance compared to OSSB generation using 90° hybrid coupler and DP-DDMZM. An improvement of 0.48 dB compared to 90° hybrid coupler and 7.41 dB compared to DP-DDMZM is observed in peak value of SNR.

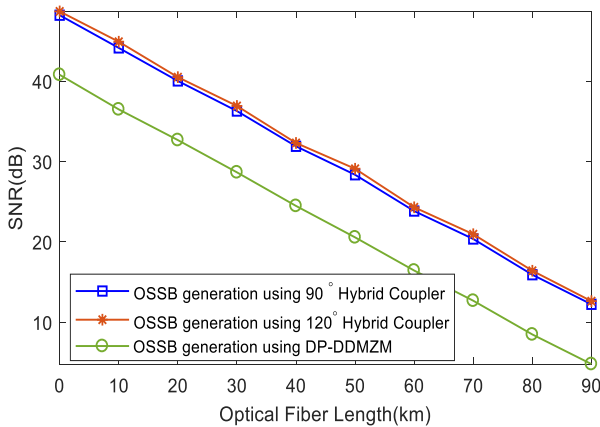


Fig. 3: SNR versus optical fiber length for OSSB generation.

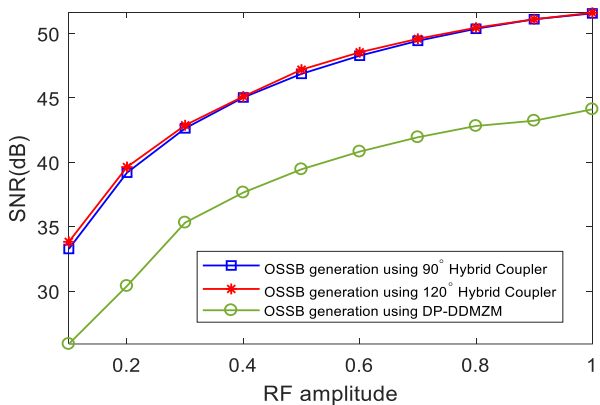


Fig. 4: SNR versus RF amplitude for OSSB generation.

The variation of received SNR with RF amplitude for OSSB generation using 90°, 120° hybrid coupler

and DP-DDMZM is shown in Fig. 4. Results are calculated for fixed 10 MHz CW laser linewidth and 20 km SMF length. Results show that as RF amplitude increases, SNR also increases. RF amplitude increases such that phase noise of the RF oscillator does not affect SNR much. It may be noted that the value of SNR is improved in OSSB generation using 120° hybrid coupler by 0.55 dB and 8 dB compared to 90° and DP-DDMZM, respectively.

The variation of received SNR with CW laser linewidth for OSSB generation using 90°, 120° hybrid coupler and DP-DDMZM is shown in Fig. 5. The value of CW laser linewidth is varied from 5 MHz to 700 MHz [9]. The plots are obtained at fixed SMF length of 20 km and RF amplitude is 0.22.

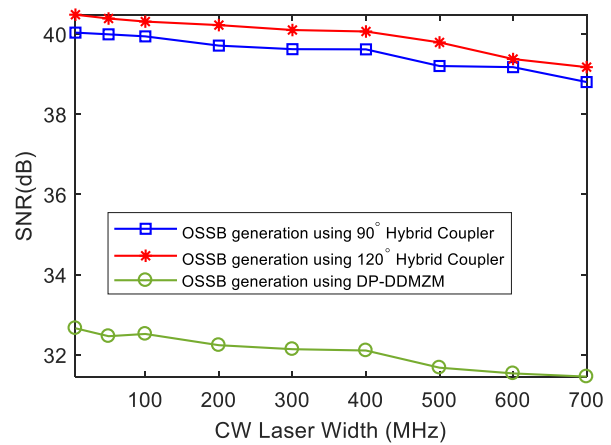


Fig. 5: SNR versus CW Laser width for OSSB generation.

The SNR decreases as CW laser line width increases. It has been observed that 120° hybrid coupler is giving improved SNR of 0.45 dB compared to 90° and 8.2 dB compared to DP-DDMZM at 5 MHz. Also, SNR of DP-DDMZM reduced to zero at higher CW laser linewidth.

4. Conclusion

Optical Single Sideband (OSSB) generation based on distinct phase angle of hybrid coupler and DP-DDMZM are compared and analyzed. In this paper, OSSB generation with and without second-order sidebands for RoF is presented. The SNR variations due to various parameters like optical fiber length, RF amplitude and laser linewidth have been investigated. The peak SNR decreases as CW laser linewidth increases in all cases. The DP-DDMZM-based systems are not suitable for higher linewidths. Further, the SNR reduces with increase in length of fiber, while increasing RF amplitude leads to increase in SNR. Elimination of one of the second-order sidebands for generating OSSB with 120° hybrid coupler gives better performance in

terms of SNR which makes them suitable for long-haul communication.

Acknowledgment

We express our gratitude to Jaypee Institute of Information Technology, 201309 Noida, India for providing research lab and tools to perform experimental work.

Author Contributions

P.G. developed theoretical formalism, performed the analytic calculations and performed the numerical simulations. Both P.G. and R.K. contributed to the final version of the manuscript. R.K. supervised the work done.

References

- [1] Fernando, X. N. *Radio Over Fiber for Wireless Communications: From Fundamentals to Advanced Topics*. 1st ed. Hoboken: Wiley, 2014. ISBN 978-1-118-79706-8.
- [2] THOMAS, V. A., M. EL-HAJJAR and L. HANZO. Millimeter-Wave Radio Over Fiber Optical Upconversion Techniques Relying on Link Nonlinearity. *IEEE Communications Surveys & Tutorials*. 2016, vol. 18, iss. 1, pp. 29–53. ISSN 1553-877X. DOI: 10.1109/COMST.2015.2409154.
- [3] SUN, J., L. YU and Y. ZHONG. A single sideband radio-over-fiber system with improved dynamic range incorporating a dual-electrode dual-parallel Mach-Zehnder modulator. *Optics Communications*. 2015, vol. 336, iss. 1, pp. 315–318. ISSN 0030-4018. DOI: 10.1016/j.optcom.2014.10.022.
- [4] ZHANG, R., J. MA, W. LIU, W. ZHOU and Y. YANG. A multi-band access radio-over-fiber link with SSB optical millimeter-wave signals based on optical carrier suppression modulation. *Optical Switching and Networking*. 2015, vol. 18, iss. 3, pp. 235–241. ISSN 1573-4277. DOI: 10.1016/j.osn.2015.08.002.
- [5] PALOI, F. and S. HAXHA. Comparative analysis of long-haul system based on SSB modulation utilising dual parallel Mach-Zehnder modulators. *Optical and Quantum Electronics*. 2018, vol. 50, no. 104, pp. 1–16. ISSN 0306-8919. DOI: 10.1007/s11082-018-1365-8.
- [6] LI, Z., H. CHI, X. ZHANG and J. YAO. Optical Single-Sideband Modulation Using a Fiber-Bragg-Grating-Based Optical Hilbert Transformer. *IEEE Photonics Technology Letters*. 2011, vol. 23, iss. 9, pp. 558–560. ISSN 1941-0174. DOI: 10.1109/LPT.2011.2116114.
- [7] SHARMA, V., A. SINGH and A. K. SHARMA. Simulative investigation on the impact of laser-spectral width in single-tone radio-over-fiber transmission system using optical single sideband technique. *Optics and Lasers in Engineering*. 2009, vol. 47, iss. 11, pp. 1145–1149. ISSN 0143-8166. DOI: 10.1016/j.optlaseng.2009.06.012.
- [8] XUE, M., S. PAN and Y. ZHAO. Optical Single-Sideband Modulation Based on a Dual-Drive MZM and a 120° Hybrid Coupler. *Journal of Lightwave Technology*. 2014, vol. 32, iss. 19, pp. 3317–3323. ISSN 1558-2213. DOI: 10.1109/JLT.2014.2344853.
- [9] KUMAR, P., S. KUMAR SHARMA and S. SINGLA. Performance analysis of an OSSB RoF link using 90° & 120° Hybrid coupler. *Optics Communications*. 2016, vol. 373, iss. 1, pp. 114–118. ISSN 0030-4018. DOI: 10.1016/j.optcom.2015.09.081.
- [10] CHAN, E. H. W., C. HUANG and C. B. ALBERT. Optical Single Sideband Modulator Without Second-Order Sidebands. *IEEE Photonics Journal*. 2018, vol. 10, iss. 3, pp. 1–10. ISSN 1943-0655. DOI: 10.1109/JPHOT.2018.2835810.
- [11] PATEL, D., V. K. SINGH and U. D. DALAL. Performance analysis of single sideband modulation technique using Mach Zehnder Modulator based on different phase angles of electrical hybrid coupler. *Optik*. 2017, vol. 128, iss. 1, pp. 93–100. ISSN 0030-4026. DOI: 10.1016/j.ijleo.2016.10.002.
- [12] PATEL, D., V. K. SINGH and U. D. DALAL. Assessment of Fiber Chromatic Dispersion Based on Elimination of Second-Order Harmonics in Optical OFDM Single Sideband Modulation Using Mach Zehnder Modulator. *Fiber and Integrated Optics*. 2016, vol. 35, iss. 4, pp. 181–195. ISSN 0146-8030. DOI: 10.1080/01468030.2016.1195899.

About Authors

Pooja GOEL received her B.Tech. from Uttar Pradesh Technical University (UPTU) and M.Tech. from Guru Gobind Singh Indraprastha University (GGSIPU), India in Electronics and Communication

Engineering, in 2005 and 2012 respectively. She is pursuing Ph.D. from Jaypee Institute of Information Technology (JIIT), Noida, India. Presently she is working as Patent Analyst doing training on Intellectual Property Rights (IPR) and related matters under the Women Scientists Scheme (WOS-C) Knowledge Involvement in Research Advancement through Nurturing (KIRAN-IPR), 11th Batch Technology Information, Forecasting & Assessment Council (TIFAC).

Rahul KAUSHIK received his B.Tech. (Electronics and Telecommunication Engineering)

and M.Tech. (Electronics Engineering) from University of Allahabad, India in 2001 and 2003 respectively. He received his Ph.D. Degree from Jaypee Institute of Information Technology (JIIT), Noida, India in 2017. Presently, he is working as Assistant Professor (Senior Grade) in the department of Electronics & Communication Engineering (ECE) at JIIT, Noida, India. His research interests lie in the areas of Optical Communication. He is a member of Optical Society (OSA), senior member of Institute of Electrical and Electronics Engineers (IEEE) and a fellow of Institution of Electronics and Telecommunication Engineers (IETE), India.